A Metric for the Quantification of Memory Effects in Power Amplifiers

João Paulo Martins, *Student Member, IEEE*, Pedro Miguel Cabral, *Student Member, IEEE*, Nuno Borges Carvalho, *Senior Member, IEEE*, and José Carlos Pedro, *Senior Member, IEEE*

***Abstract*—This paper presents a quantitative metric for memory effects in power amplifiers (PAs) and applies it to various active device technologies and wireless system contexts. The proposed metric is mathematically founded in the dynamic two-tone distortion response, has a clear physical meaning in the important field of PA linearization and can be easily evaluated from either harmonic balance simulations or measurement data gathered in a microwave laboratory. In addition, a memoryless PA linearizer, optimum for reducing the integrated intermodulation distortion (IMD) power in the operation bandwidth for a two-tone excitation, is derived, providing a rigorous figure-of-merit of PA linearizability under static IMD compensation. The application of this figure-of-merit is then illustrated for three different PA prototypes based on Si LDMOS, InGaP/GaAs heterojunction bipolar transistors, and GaN high electron-mobility transistors, designed for 900-MHz (global system for mobile communications), 2.1-GHz (wideband code division multiple access), and 3.5-GHz (WiMax) wireless systems, respectively.**

***Index Terms*—Long-term memory, memory effects (MEs), nonlinear systems, power amplifiers (PAs).**

I. Introduction

MEMORY effects (MEs) have a strong impact on wireless communication systems performance since they increase the error vector magnitude of their modulation schemes. Moreover, they are known to impair most common (memoryless) power amplifier (PA) linearization techniques. As a result, they have been receiving a large amount of attention from PA design engineers.

MEs can be subdivided into two different types of phenomena according to the time constants involved. Short-term MEs address time constants of the order of the carrier period and are caused by both the reactive components of the active device and matching networks at the RF band. Since these time constants are much smaller than the ones involved in the information time scale, their effects can be considered as static and the corresponding PAs memoryless.

Manuscript received March 31, 2006; revised June 30, 2006. This work was supported in part by the European Union under the Network of Excellence TARGET Contract IS-1-507893-NoE and under Project ColteMepai POSC/EEA-ESE/55739/2004. The work of J. P. Martins was supported by the Portuguese Science Foundation Fundação para a Ciência e Tecnologia under Ph.D. Grant 22056/2005. The work of P. M. Cabral was supported by the Portuguese Science Foundation Fundação para a Ciência e Tecnologia under Ph.D. Grant 11323/2002.

The authors are with the Instituto de Telecomunicações, Universidade de Aveiro, 3810-193 Aveiro, Portugal (e-mail: joaoptm@av.it.pt; pcabral@av.it.pt; nborges@det.ua.pt; jcpedro@ieee.org).

Digital Object Identifier 10.1109/TMTT.2006.882871

In contrast, long-term MEs are low-frequency phenomena (from dc to a few kilohertz or megahertz) involving time constants that are comparable to the information time scale, thus pressing dynamic effects onto the signal's envelope. They are usually attributed to the active device's dynamic thermal effects (i.e., involving some sort of thermal inertia), the active device's charge carrier traps, or to the biasing networks [1], [2].

From a behavioral point-of-view, both MEs show up as hysteresis in the AM/AM and AM/PM plots, or as different two-tone intermodulation responses for varying tone spacing [3].

In practice, these MEs play a key role in the PA linearization field since they decrease the performance of most widely used linearization schemes [1], [5]. Considering that traditional PA linearizers are designed as memoryless devices, they are ineffective in the presence of IMD dynamics, having no profitable effect on reducing the PAs' distortion power. This is so important that the microwave PA industry has been asking for some form of ME metric capable of evaluating the PA linearizability.

A first attempt to answer this question was addressed by Moulthrop *et al.* in [5] and Ku *et al.* in [6]. In those studies, the authors assumed that the best memoryless linearizer (BML) was the one that exactly compensates the measured PA AM/AM–AM/PM characteristics. The authors then defined a metric for memoryless PA linearization as the normalized ratio between the AM/AM–AM/PM response and the deviations of the actual PA two-tone intermodulation distortion (IMD) from this AM/AM–AM/PM baseline. Although useful, this metric has been difficult to apply in the industrial environment due to two main reasons.

First, it was conceived and defined under the development of a PA parallel Wiener behavioral model [6]. This gives the impression that it can only be applied after model extraction. Second, and most important, it relies on the assumption that the BML is the one obtained from the AM/AM–AM/PM characteristics. Effectively, if we recognize that these characteristics are the extrapolated two-tone IMD when the tone separation tends to zero, and considering that the main source of PA MEs is the inductive bias circuitry, we immediately conclude that such a linearizer is not the best among all the possible memoryless implementations.

In this paper, an in-depth extension of the concept presented in [7] is given, and the BML theory for a two-tone excitation is revisited. Using the two-tone IMD data obtained after the application of this BML, a new figure-of-merit was proposed for quantifying MEs in PAs, which also provides a measure of the PA maximum memoryless linearizability.

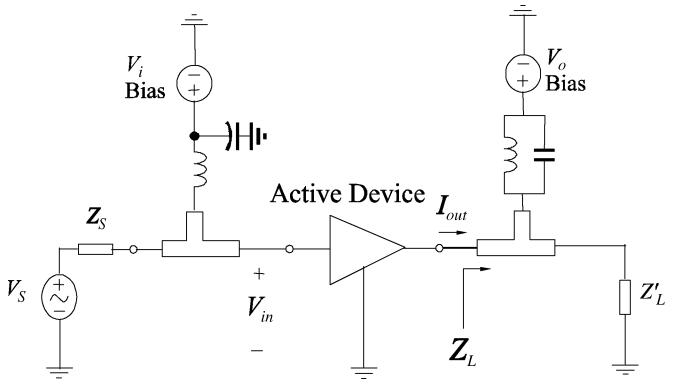

Fig. 1. FET-based PA equivalent-circuit diagram used for the theoretical analysis.

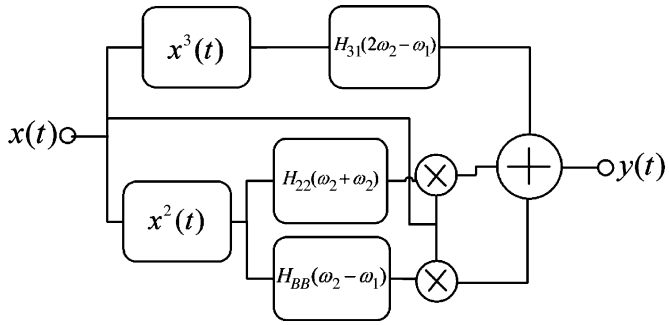

Fig. 2. Model for the PA's long-term memory mechanisms.

To achieve this goal, the two-tone IMD response is first measured over the operation envelope bandwidth. This equivalent frequency-domain nonlinear transfer function is then converted into a time-domain impulse response, leading to a physical interpretation of the metric's ability to actually characterize the MEs. Finally, this theory is illustrated through its application to different practical PA prototypes.

This paper will thus be organized as follows. First, the BML theory and the memory figure-of-merit (MFOM) definition are presented and discussed in detail with its validity addressed by simulation. We then move to the characterization of an in-house built Si LDMOS PA specially designed to include controllable MEs via an appropriate modification of its bias networks. Next, two different commercial PAs—a WCDMA [8] InGaP/GaAs heterojunction bipoloar transistor (HBT) PA and a WiMax [9] GaN high electron-mobility transistor (HEMT) PA—are measured and evaluated for their MEs. Note that these results are not meant for any form of comparison between the different PAs—since they were based on different device technologies and conceived for distinct wireless environments—but rather to show the characterization capability of the proposed MFOM for real commercial PAs. Finally, the paper ends summarizing the key conclusions of the developed work.

II. Long-Term MFOM Revisited

In [7], a new figure-of-merit concept for the evaluation of PA MEs was proposed enabling the comparison between the linearizability of different PAs. In order to provide a clearer understanding of this MFOM, we first start with a discussion of the MEs mechanisms arising in a nonlinear PA.

Fig. 1 shows the PA circuit schematic used to model a generic field-effect transistor (FET)-based PA.

Using a Volterra-series description, it is possible to relate the IMD behavior with the PA circuit components. Since this type of analysis is well known from previous publications [2], [10], only the third-order IMD transfer function, which corresponds to the spectral regrowth at $2\omega_2 - \omega_1$, will be presented in (1), shown at the bottom of this page, where

$$H_2(\omega_1,\omega_2) = \frac{G_{m2} - 1/2G_{md}\left[H_1(\omega_1)Z_L(\omega_1) + H_1(\omega_2)Z_L(\omega_2)\right]}{\left[1 + G_{ds}Z_L(\omega_1+\omega_2)\right]} \tag{2}$$

and

$$H_1(\omega) = \frac{G_m}{\left[1 + G_{ds}Z_L(\omega)\right]}. \tag{3}$$

From this simple model, it is easily seen that the output third-order IMD will comprise three different components: one is a direct term arising from G_{m3} that does not depend on $\omega_2 - \omega_1$; a second-order term arising from the $(\omega_1 + \omega_2)$ band, which also does not depend on $\omega_2 - \omega_1$; and finally a term that can be interpreted as an up-conversion of the baseband components back to the fundamental frequencies. This can be represented by the model shown in Fig. 2 [11] where

$$H_{31}(2\omega_2 - \omega_1) = \frac{G_{m3}}{1 + G_{ds}Z_L(2\omega_2 - \omega_1)} \tag{4}$$

$$H_{22}(\omega_2 + \omega_2) = \frac{-1/3G_{md}H_2(\omega_2,\omega_2)Z_L(2\omega_2)}{1 + G_{ds}Z_L(2\omega_2 - \omega_1)} \tag{5}$$

and

$$H_{BB}(\omega_2 - \omega_1) = \frac{-2/3G_{md}H_2(\omega_2,-\omega_1)Z_L(\omega_2,-\omega_1)}{1 + G_{ds}Z_L(2\omega_2 - \omega_1)}. \tag{6}$$

Assuming that this PA model is excited by a frequency-domain input signal $x(t) \rightarrow X(\omega)$, the output IMD at $2\omega_2 - \omega_1$ is given by

$$\begin{aligned} Y(2\omega_2-\omega_1) = {} & H_{31}(2\omega_2-\omega_1)X(\omega_2)X(\omega_2)X(\omega_1)^* \\ & + X(\omega_1)^*[H_{22}(2\omega_2)X(\omega_2)X(\omega_2)] \\ & + X(\omega_2)[2H_{BB}(\omega_2-\omega_1)X(\omega_2)X(\omega_1)^*]. \end{aligned} \tag{7}$$

$$H_3(\omega_2,\omega_2,-\omega_1) = \frac{G_{m3} - 1/3G_{md}\left[2H_2(\omega_2,-\omega_1)Z_L(\omega_2-\omega_1) + H_2(\omega_2,\omega_2)Z_L(\omega_2+\omega_2)\right]}{\left[1 + G_{ds}Z_L(2\omega_2-\omega_1)\right]} \tag{1}$$

If we consider $H_{22}(.)$ and $H_{31}(.)$ to be constant with $\Delta\omega = \omega_2 - \omega_1$, then the output IMD variation will only depend on $H_{BB}(\Delta\omega)$ and, thus, this term will be the exclusive source for the PA long-term MEs. This assumption is reasonable since, as $\Delta\omega$ varies from dc up to a few megahertz, the baseband frequency will vary for some decades, while the second harmonic and the fundamental will only vary a small percentage of the center frequency. This $H_{BB}(\Delta\omega)$ variation can be attributed to baseband impedance, which occurs, for instance, due to bias networks, thermal effects, or trapping. In fact, the most striking factor for the baseband impedance variation is the bias networks, as previously presented in [2].

Important information can be gathered from this model that can be summarized as follows:

- First, if any of the $H_{31}(.)$ or $H_{22}(.)$ terms is significantly larger than the one involving $H_{BB}(.)$, we can be misled by the fact that variation in IMD with $\Delta\omega$ may not be evident, although the PA still presents MEs that will impair the performance of a memoryless linearizer.
- Second, the IMD asymmetry (different upper and lower IMD components at $2\omega_2 - \omega_1$ and $2\omega_1 - \omega_2$, respectively) only appears when both output impedances at $\omega_2 - \omega_1$ and $\omega_2 + \omega_1$ are complex. In this simple model, this implies that either the in-band direct path or the second harmonic path contributes with a certain amount of imaginary values [2]. This provides a strong insight into these problems since it states that we can have long-term MEs even without IMD asymmetry.

One way or the other, the impact of MEs in the PA will limit the use of memoryless linearizers. That is due to the fact that, in a memoryless linearizer, the upper band IMD is necessarily equal to the lower band one, and cannot track any IMD variation with frequency shown by the PA. In the dynamic IMD case, the upper band is

$$Y(2\omega_2 - \omega_1) = K + 2H_{BB}(\omega_2 - \omega_1)X(\omega_2)X(\omega_2)X(\omega_1)^* \tag{8}$$

and the lower band becomes

$$Y(2\omega_1 - \omega_2) = K + 2H_{BB}(\omega_2 - \omega_1)^*X(\omega_1)X(\omega_1)X(\omega_2)^* \tag{9}$$

where K is a complex quantity that is constant over the tone spacing.

If we now realize that $X(\omega_1) = X(\omega_2)$, then the difference between the two IMD sidebands come from the addition or subtraction of the imaginary parts of $H_{BB}(\Delta\omega)$ and K, which will imply a different upper and lower IMD value. In order to account for this IMD variation over the operating bandwidth, we should recognize that the term $H_{BB}(\Delta\omega)$ is of foremost importance since it is the only one that depends on frequency spacing. Indeed, for capturing those desired MEs, we should neglect the constant part of (8) and (9), and retain the only one that changes with the envelope frequency. In (7), the constant part corresponds to $H_{31}(.)$ and $H_{22}(.)$, thus, after the cancellation, only $H_{BB}(\omega_2 - \omega_1)$ will be obtained. This will lead us to the conclusion that although the two-tone IMD must, in general, be modeled through a three-dimensional nonlinear transfer function, it can also be represented via a one-dimensional frequency-domain transfer function of the tone spacing $\Omega \equiv \Delta\omega$. In fact, this is the same assumption behind the widely adopted first-order dynamics truncation of the nonlinear integral model [12] or the nonlinear impulse response model [13]. Moreover, it should be said that a swept $\Delta\omega$ two-tone test of a PA around the operating central frequency implicitly assumes this one-dimensional nature. Thus, (7) can be viewed as $Y(2\omega_2 - \omega_1) = Y_{\mathrm{IM3}}(\Omega) = Y(\omega_2 + \Delta\omega)$, which is the measured (or, possibly, calculated) PA two-tone response used for defining the new ME metric.

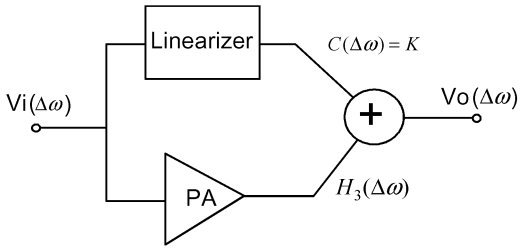

Fig. 3. General PA linearization arrangement.

The next step consists of defining the best two-tone memoryless linearizer (i.e., the BML) of the PA. For that, we assume the general block diagram depicted in Fig. 3, in which the linearizer is used to generate an auxiliary IMD that will compensate the one produced by the standalone PA.

Note that although Fig. 3 uses a feed-forward topology, it can be easily applied to any cascade (pre- or post-distortion) or feedback arrangement, as the output adder does not necessarily stand for any output signal coupler, but for the conceptual addition (in fact, subtraction) of the IMD produced by the PA and its linearizer.

Under this conceptual linearization scheme, we now define the BML for a given PA as the static (or constant with frequency Ω) auxiliary device of Fig. 3 that produces a constant (with tone-spacing) two-tone IMD response C that minimizes the distortion power in the considered operation bandwidth W[1]

$$C: \left[\int_{-W}^{+W} |C - Y_{\mathrm{IM3}}(\Omega)|^2 \, d\Omega\right] \text{ is minimum.} \tag{10}$$

From a mathematical viewpoint, this expression states that our memoryless linearizer is a mean square-error constant estimator, which can thus be determined by

$$\frac{\partial}{\partial C}\left[\int_{-W}^{+W} |C - Y_{\mathrm{IM3}}(\Omega)|^2 \, d\Omega\right] = 0$$

$$\Rightarrow C = \frac{1}{2W}\int_{-W}^{+W} Y_{\mathrm{IM3}}(\Omega) d\Omega. \tag{11}$$

Therefore, the optimum memoryless linearizer of a certain PA (in a two-tone IMD sense) is nothing more than the system whose constant response is the vectorial mean of the response of that PA to a swept envelope frequency two-tone test $Y_{\mathrm{IM3}}(\Omega)$ within the bandwidth of interest. This constant response can

[1]Note that, although the following discussion is handled in terms of the actual response, not the transfer function as is more usual, one is easily converted into the other because the response to a unity complex exponential (a unity impulse) is numerically equal to the frequency-domain transfer function (the time-domain impulse response).

be easily estimated in a microwave laboratory by measuring $Y_{\mathrm{IM3}}(\Omega)$ in amplitude and phase over the desired bandwidth.

To get a deeper insight into what such an optimum memoryless linearizer would be, we now turn to the time domain. For that, we perform the inverse Fourier transform of $Y_{\mathrm{IM3}}(\Omega)$ of (11) to obtain

$$C = \frac{1}{2W}\int_{-W}^{+W}\left[\int_{0}^{\infty} y_{\mathrm{IM3}}(\tau)e^{-j\Omega\tau}d\tau\right]d\Omega = \int_{0}^{\infty} y_{\mathrm{IM3}}(\tau)\mathrm{sinc}(W\tau)d\tau \tag{12}$$

where $\mathrm{sinc}(x) \equiv \sin(x)/x$.

Two limiting situations of the tested $Y_{\mathrm{IM3}}(\Omega)$ can be studied. First, we will impose no restriction on the bandwidth, letting $W \to \infty$. In this case, $\mathrm{sinc}(W\tau)$ becomes a very narrow function (a Dirac delta function) around zero and (12) gives $C = y_{\mathrm{IM3}}(0)$. This means that the optimum memoryless linearizer is such that it cancels out the PA instantaneous (or memoryless) IMD, exactly what we were expecting it to do.

Now we consider the opposite situation in which $W \to 0$. This is the case where C is made equal to $Y_{\mathrm{IM3}}(0)$, i.e., the AM/AM–AM/PM characteristics. The function $\mathrm{sinc}(W\tau)$ is now a very wide and flat function, and C becomes

$$C = \int_{0}^{\infty} y_{\mathrm{IM3}}(\tau)d\tau \tag{13}$$

the average of the $y_{\mathrm{IM3}}(t)$ impulse response tail.

Thus, the AM/AM–AM/PM linearizer can only be optimum whenever the amplifier is processing a signal whose envelope bandwidth is much smaller than the PA swept tone spacing IMD characteristics or the temporal IMD dynamics are much slower than the PA memory span.

III. Simulated Impulse Response of the BML

In order to get a deeper understanding of the BML concept, a harmonic-balance simulation was conducted on a simplified PA circuit based on a memoryless transistor model. However, two different bias networks were considered in order to produce different, but controllable MEs.

A two-tone signal was then used as the input excitation and the output IMD was obtained in magnitude and phase as a function of the input tone separation (see Figs. 4 and 5, respectively).

As expected, in the memoryless case, there are no visible changes in both IMD magnitude and phase plots, while in the dynamic case, a large variation with tone spacing is clearly seen. Moreover, the phase shown in Fig. 5 is always zero for the memoryless PA, and something else (not even necessarily antisymmetrical) when the PA presents memory.

Following the formulation presented in Section II, the BML can be determined from the impulse response's first coefficient $C = y_{\mathrm{IM3}}(0)$, which is equivalent to the average amplitude and phase IMD frequency variation presented in Figs. 4 and 5, respectively.

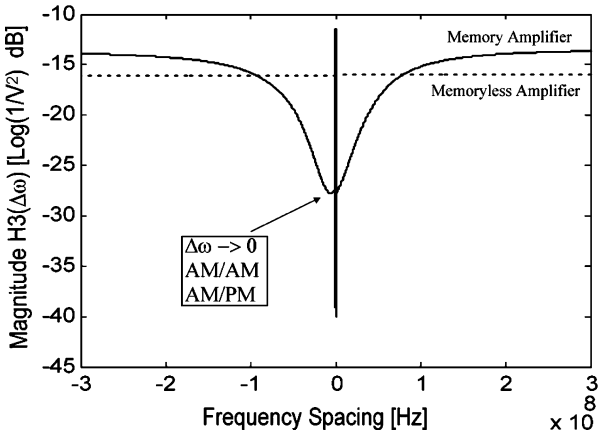

Fig. 4. Simulated IMD magnitude for the memoryless PA and for the PA presenting memory.

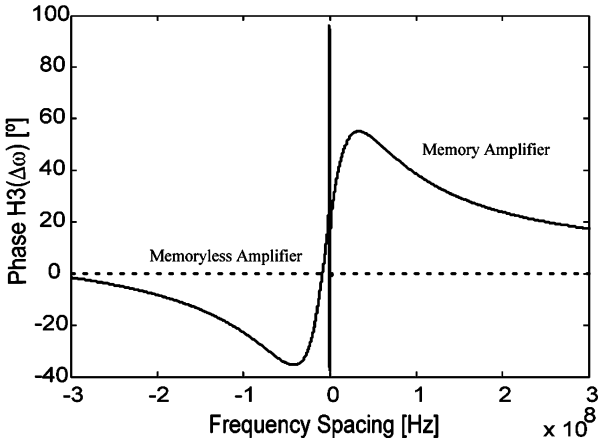

Fig. 5. Simulated IMD phase for the memoryless PA and for the PA presenting memory.

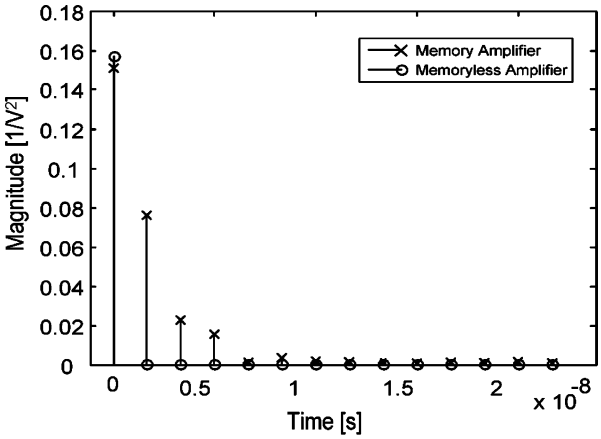

Fig. 6. Impulse response magnitude for the memoryless PA and for the PA presenting memory.

The impulse response in the memoryless case is a single Dirac delta function at the time origin (see Fig. 6), while in the dynamic case, it expands throughout a certain time span, as expected.

One interesting thing to point out is the complex nature of the obtained impulse response, i.e., that it presents a nonnull imaginary part or a phase that can be something other than 0° or 180°, as shown in Fig. 7. Mathematically, this is a consequence of

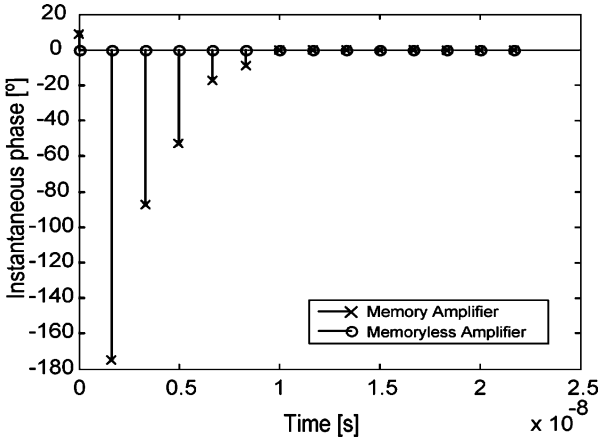

Fig. 7. Impulse response phase for the memoryless PA and for the PA presenting memory.

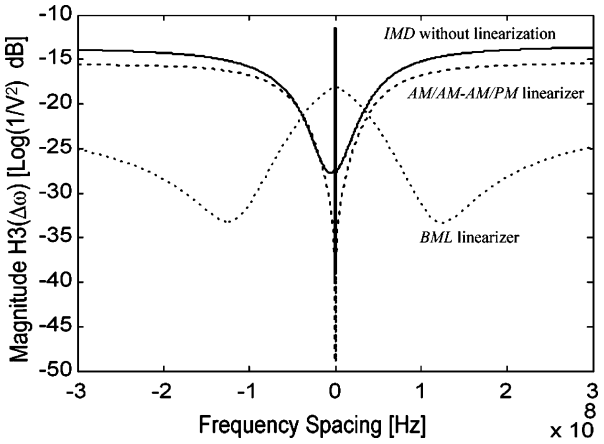

Fig. 8. Linearizability of the PA presenting memory using the AM/AM–AM/PM static linearizer and the now defined BML.

the fact that the frequency response does not present a complex conjugate symmetry with respect to $\Omega = 0$ or that the upper and lower IMD sidebands are not symmetrical (even symmetry for the amplitude and odd symmetry for the phase). Realizing that $Y_{\mathrm{IM3}}(\Omega)$ is the distortion response of the PA to a two tone, actually a double-sideband amplitude modulation with a carrier frequency $\omega_c = (\omega_1+\omega_2)/2$ and a carrier envelope of frequency $\omega_m = (\omega_1-\omega_2)/2$ cosine envelope, the amplitude and phase of our impulse response can be interpreted as the evolution in time of the transient response of the AM/AM and AM/PM behavior when the PA is subject to an excitation whose envelope is an ideal impulse. In this sense, it naturally results that the average of the $y_{\mathrm{IM3}}(t)$ amplitude is the PA's AM/AM and the nonnull average of the $y_{\mathrm{IM3}}(t)$ phase is the PA's AM/PM.

Now we compare the performance of our BML with that of the AM/AM–AM/PM static linearizer, respectively, obtained from the simulated $Y_{\mathrm{IM3}}(\Omega)$ average and the limit of the IMD response when Ω tends to zero for the dynamic amplifier. Fig. 8 presents the linearizability of the PA presenting memory when both linearizers are used.

As can be seen in Fig. 8, the improved quality of the proposed BML approach lies on the better average linearization obtained along the frequency band when compared with the AM/AM–AM/PM static linearization technique. This directly

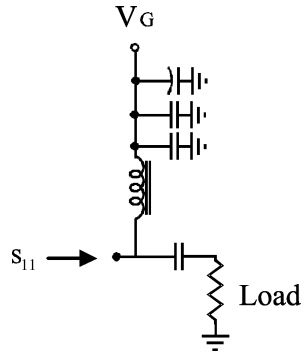

Fig. 9. Bias network used in the Si LDMOS-based PA design.

results from the way the new BML was defined, which is, indeed, optimum for the selected excitation: the standard two-tone stimulus.

IV. MFOM for Long-Term MEs

After the explanation of the BML, we are now in a position to define the MFOM of PA linearizability under static conditions [7]. Intuitively this metric should measure the ratio between the unlinearized IMD integrated power in the desired bandwidth and the total IMD integrated power after memoryless linearization in the same bandwidth[2]

$$L_M = \frac{\int_{-W}^{+W} |Y_{\mathrm{IM3}}(\Omega)|^2 \, d\Omega}{\int_{-W}^{+W} |Y_{\mathrm{IM3}}(\Omega) - C|^2 \, d\Omega}. \tag{14}$$

Although defined and explained in the frequency domain, such an MFOM can reveal an even more interesting significance when seen in the time domain. For that, we consider again the case where we are interested in the whole PA IMD bandwidth characteristics, i.e., $W \to \infty$. Since in that case, $C = y_{\mathrm{IM3}}(0)$, Parseval's theorem states that our MFOM actually is a metric of the power contained only in the PA dynamic IMD, normalized to the total IMD power. Thus, L_M in (14) is indeed a metric of PA long-term MEs.

V. In-House Si-LDMOS PA Evaluation

In order to validate the proposed theoretical results, a 5-W 900-MHz Si-LDMOS-based PA for global system for mobile communications (GSM) applications [14] was carefully designed using two different bias networks: one memoryless and another one presenting memory in the bandwidth of interest. Fig. 9 presents the generic schematic for both proposed networks.

The memoryless bias network was designed to be close to a short circuit in the entire frequency span, while the bias network for dynamic behavior was conceived to present a variable frequency response at baseband.

The baseband impedances shown by these two bias networks are depicted in Fig. 10.

A two-tone excitation signal was chosen for both the memoryless and dynamic PA, and the center frequency was set to 900 MHz. The tone frequency separation ranged from 4 kHz to

[2]The figure-of-merit definition herein given is the inverse of the one presented in [8] since, this way, it can be more easily interpreted as a metric of the system's linearizability.

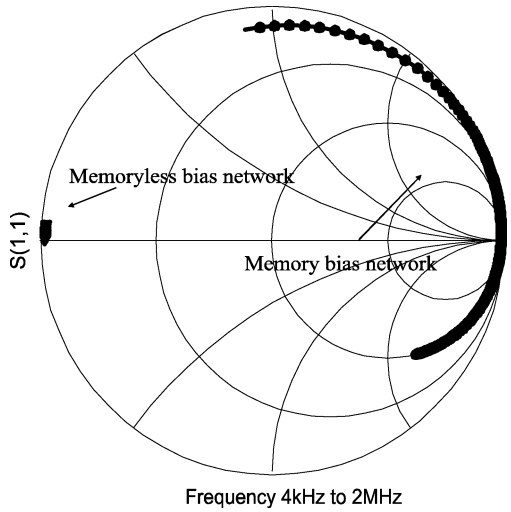

Fig. 10. Measured S_{11} of the bias network.

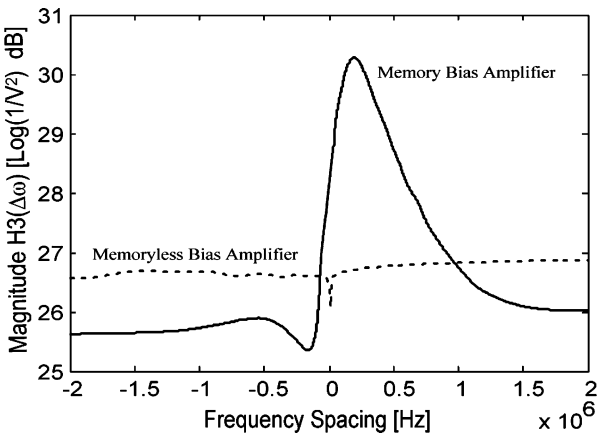

Fig. 11. Measured magnitude values of the third-order transfer function $H_3(\Delta\omega)$.

2 MHz [15]. Figs. 11 and 12 present the measured magnitude and phase values of the one-dimensional third-order transfer function $H_3(\Delta\omega)$ for both bias network cases.

From Figs. 11 and 12, it can be seen that the memoryless PA presents an almost flat magnitude response and a linear phase variation. The corresponding impulse response, obtained from the inverse Fourier transformation of $H_3(\Delta\omega)$, is presented in Figs. 13 and 14, and matches a single Dirac delta defining the BML, as was theoretically predicted.

After the linearization procedure using the BML, the IMD ratio results where compared with the ones obtained before linearization.

Looking at the third-order intermodulation ratio (IMR), the linearized response presented in Fig. 15, a residual value of IMR variation can be observed. This could be attributed to dynamic phenomena other than the one determined by the bias networks (e.g., thermal effects). The good performance of the memoryless PA can be seen from the 22.3-dB MFOM obtained.

In the dynamic PA case (Figs. 11 and 12), the magnitude and phase of $H_3(\Delta\omega)$ shows a variation with frequency spacing that even includes some asymmetry. The impulse response now obtained is no longer a single Dirac delta at $t = 0$, but expands through a certain memory span, but similar to what was done

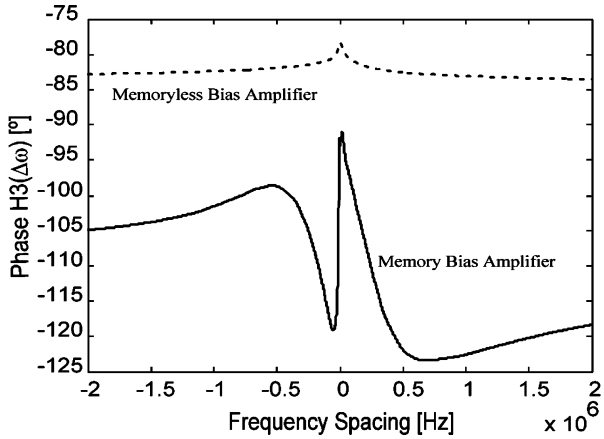

Fig. 12. Measured phase values of the third-order transfer function $H_3(\Delta\omega)$.

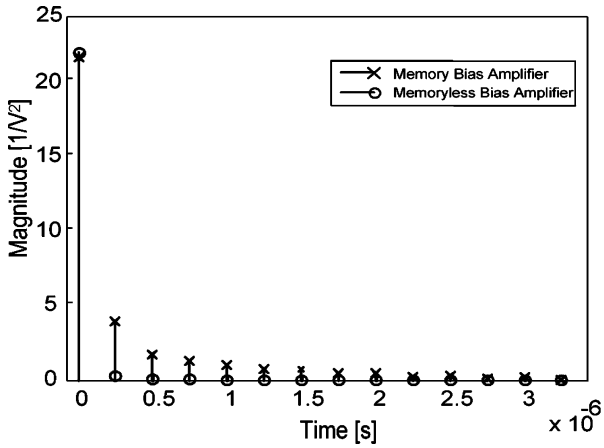

Fig. 13. Measured magnitude values of the third-order transfer function impulse response $h_3(\tau)$.

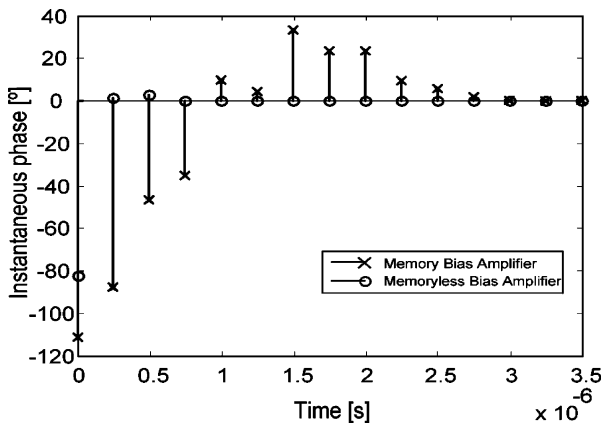

Fig. 14. Measured phase values of the third-order transfer function impulse response $h_3(\tau)$.

before, the BML was still obtained from only the instantaneous value of this response (refer to Figs 13 and 14). After this linearization procedure, the IMR results were once again compared with the ones obtained before linearization, as shown in Fig. 16. A visible variation in the IMR response can be noticed both in the linearized and nonlinearized tests.

As expected, the memoryless linearizability is now much lower than the one measured for the memoryless PA, as quantified by the obtained 7.6-dB MFOM.

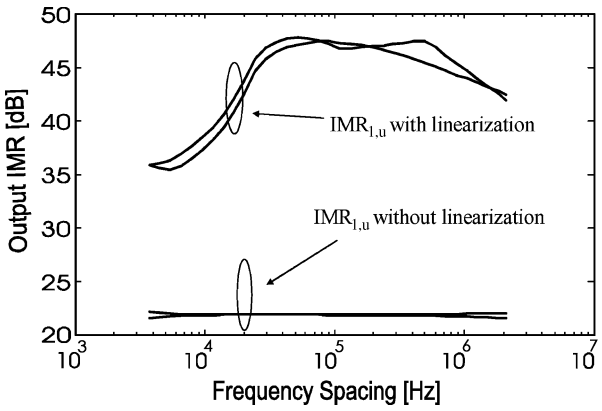

Fig. 15. Measured results of the memoryless Si-LDMOS-based PA before linearization and after linearization with the BML for both upper and lower sidebands.

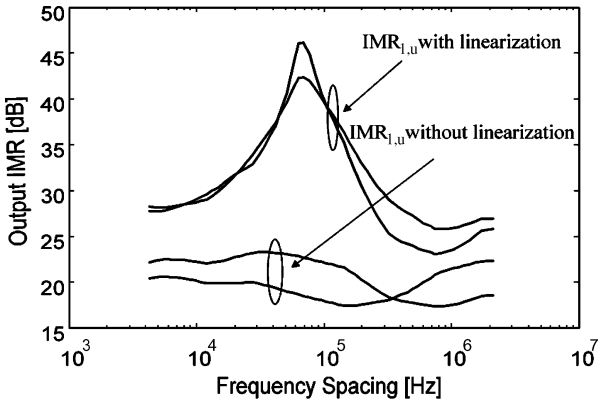

Fig. 16. Measured results of the Si-LDMOS-based PA presenting memory before linearization and after linearization with the BML for both upper and lower sidebands.

These results show that the MEs appearing in this PA, due to the bias networks, indeed severely degrade the memoryless linearizability of the proposed design.

VI. MFOM Evaluation for Commercial PAs

In order to prove the applicability of this new MFOM in real scenarios, the same procedure was followed using two commercial PAs developed for different wireless system applications. The first PA used was a 1.5-W 2.14-GHz InGaP/GaAs HBT-based PA designed for W-CDMA systems [8]. The input excitation used was a two-tone signal with varying tone separation, again, from 4 kHz to 2 MHz. Fig. 17 presents the IMR values obtained before and after the described memoryless linearization procedure.[3]

In this case, a high value of linearizability could be achieved with this amplifier, expressed by the 24.5-dB MFOM obtained.

The second PA used was a 2-W 3.5-GHz GaN HEMT-based PA, intended for WiMax [9] applications. Fig. 18 presents the IMR values obtained before and after the linearization procedure.

In this case, a MFOM of 27 dB was achieved, again stating a high value of memoryless linearizability for this PA.

[3]Since the purpose of this experimental section is to demonstrate the ability of the proposed figure-of-merit to capture the long-term MEs, the amplifiers were operated in a region beyond their rated specifications in order to show its validity even in limit cases.

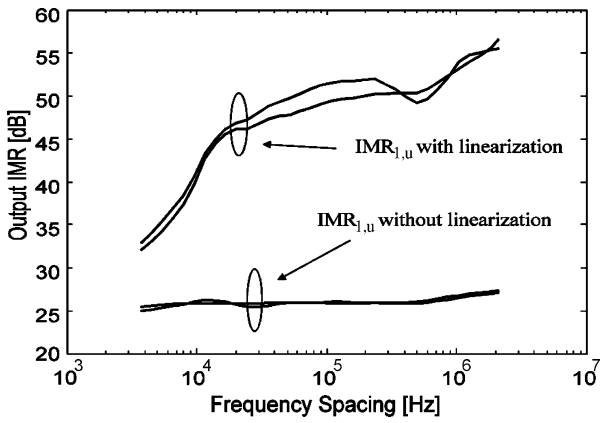

Fig. 17. Measured results of the InGaP/GaAs HBT-based PA before linearization and after memoryless linearization with the BML for both upper and lower sidebands.

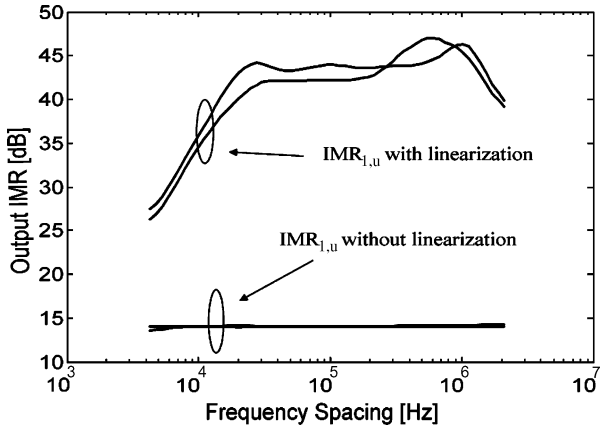

Fig. 18. Measured results of the GaN HEMT-based PA, before linearization and after linearization with the BML for both upper and lower sidebands.

VII. Conclusions

This paper has presented a metric for the quantification of MEs in PAs. The proposed metric was given as an intuitive and easily measurable MFOM, defined as the unlinearized IMD total power normalized to the IMD power obtained after optimum static linearization. When seen from the time domain, this MFOM can be extremely useful for classify PAs according to their long-term MEs and memoryless linearizability. In order to obtain this MFOM, a novel two-tone memoryless linearizer norm was also established, which proved to be the BML under two-tone excitation when compared to other previously proposed alternatives.

Finally, this PA dynamic nonlinearity characterization method was applied to various in-house and commercial PAs, demonstrating its validity.

If a PA is now evaluated using this MFOM, then its linearizability can be easily determined, thus possibly reducing the industry's time to market.

Acknowledgment

The authors wish to acknowledge the RFHIC Company Ltd., Suwon, Korea, WJ Communications Inc., San Jose, CA, and Freescale Semiconductor Inc., Tempe, AZ, for providing the amplifiers used in this study.

The authors would also like to express their gratitude to the reviewers for their comments and suggestions.

REFERENCES

[1] J. H. K. Vuolevi, T. Rahkonen, and J. P. A. Manninen, "Measurement technique for characterizing memory effects in RF power amplifiers," *IEEE Trans. Microw. Theory Tech.*, vol. 49, no. 8, pp. 1383–1389, Aug. 2001.

[2] N. B. Carvalho and J. C. Pedro, "A comprehensive explanation of distortion sideband asymmetries," *IEEE Trans. Microw. Theory Tech.*, vol. 50, no. 9, pp. 2090–2101, Sep. 2002.

[3] P. M. Cabral, J. C. Pedro, and N. B. Carvalho, "Dynamic AM–AM and AM–PM behavior in microwave PA circuits," in *Asia–Pacific Microw. Conf. Dig.*, Shangai, China, 2005, pp. 971–974.

[4] P. B. Kennington, *High-Linearity RF Amplifier Design*. Norwood, MA: Artech House, 2000.

[5] A. A. Moulthrop, C. J. Clark, C. P. Silva, and M. S. Muha, "A dynamic AM/AM and AM/PM measurement technique," in *IEEE MTT-S Int. Microw. Symp. Dig.*, Jun. 1997, vol. 3, pp. 1455–1458.

[6] H. C. Ku, M. D. McKinley, and J. S. Kenney, "Quantifying memory effects in RF power amplifiers," *IEEE Trans. Microw. Theory Tech.*, vol. 50, no. 12, pp. 2843–2849, Dec. 2002.

[7] J. P. Martins, N. B. Carvalho, and J. C. Pedro, "A figure-of-merit for the evaluation of long term memory effects in RF power amplifiers," in *IEEE MTT-S Int. Microw. Symp. Dig.*, San Francisco, CA, Jun. 2006, pp. 1109–1112.

[8] Universal Mobile Telecommunications System (UMTS) physical layer ETSI, Sophia-Antipolis, France, ETSI TS 125 215 V6.4.0, 1999.

[9] *Local and Metropolitan Area Networks*, IEEE Standard 802.16E-2005 & 802.16/COR1, 2005.

[10] J. C. Pedro and N. B. Carvalho, *Intermodulation Distortion in Microwave and Wireless Circuits*. Norwood, MA: Artech House, 2003.

[11] A. Walker, M. Steer, K. Gard, and K. Gharaibeh, "Multi-slice behavioural model of RF systems and devices," in *Radio Wireless Conf. Dig.*, Atlanta, GA, Sep. 2004, pp. 71–74.

[12] F. Filicori, G. Vannini, and V. Monaco, "A nonlinear integral model of electron devices for HB circuit analysis," *IEEE Trans. Microw. Theory Tech.*, vol. 40, no. 7, pp. 1456–1465, Jul. 1992.

[13] E. Ngoya and A. Soury, "Envelope domain methods for behavioral modeling," in *Fundamentals of Nonlinear Behavioral Modeling for RF and Microwave Design*, J. Wood and D. Root, Eds. Norwood, MA: Artech House, 2005.

[14] Digital Cellular Telecommunications System (phase 2+); physical layer on the radio path; general description ETSI, Sophia-Antipolis, France, TS 100 573 V7.1.0, 1999.

[15] J. Martins and N. Carvalho, "Multitone phase and amplitude measurement for nonlinear device characterization," *IEEE Trans. Microw. Theory Tech.*, vol. 53, no. 6, pp. 1982–1989, Jun. 2005.

João Paulo Martins (S'06) was born in Sever do Vouga, Portugal, on May 13, 1973. He received the B.Sc. and M.Sc. degrees from the Universidade de Aveiro, Aveiro, Portugal, in 2001 and 2004, respectively, and is currently working toward the Ph.D. degree in MEs in nonlinear systems at the Universidade de Aveiro.

Since 2001, he has been a Researcher with the Instituto de Telecomunicações, Universidade de Aveiro. His main interests are in wireless systems and nonlinear microwave circuit design.

Pedro Miguel Cabral (S'04) was born in Oliveira de Azemeis, Portugal, in October 1979. He received the Bs.C. degree in electrical engineering from the Universidade de Aveiro, Aveiro, Portugal, in 2002, and is currently working toward the Ph.D. degree in nonlinear transistor modeling.

He currently lectures several laboratory classes at the Universidade de Aveiro. His main interests are nonlinear modeling and design of microwave circuits and active devices.

Mr. Cabral was the recipient of the 2002 prize for the best electrical engineering student at the Universidade de Aveiro. In 2004, he was a finalist of the Student Paper Competition presented at the IEEE Microwave Theory and Techniques Society (IEEE MTT-S) International Microwave Symposium (IMS).

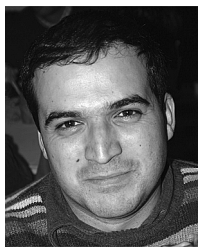

Nuno Borges Carvalho (S'92–M'00–SM'05), was born in Luanda in 1972. He received the Diploma and Doctoral degrees in electronics and telecommunications engineering from the Universidade de Aveiro, Aveiro, Portugal, in 1995 and 2000, respectively.

From 1997 to 2000, he was an Assistant Lecturer with the Universidade de Aveiro, in 2000 was a Professor, and is currently an Associate Professor. He is also a Senior Research Scientist with the Instituto de Telecomunicações, Universidade de Aveiro. He was a Scientist Researcher with the Instituto de Telecomunicações, during which time he was engaged in different projects on nonlinear computer-aided design (CAD) and circuits and RF system integration. He coauthored *Intermodulation in Microwave and Wireless Circuits* (Artech House, 2003). He has been a reviewer for several magazines. His main research interests include CAD for nonlinear circuits, design of highly linear RF-microwave PAs, and measurement of nonlinear circuits/systems.

Dr. Borges Carvalho is a member of the Portuguese Engineering Association. He is a reviewer for the IEEE TRANSACTIONS ON MICROWAVE THEORY AND TECHNIQUES and an IEEE MTT-11 Technical Committee member. He was the recipient of the 1995 Universidade de Aveiro and the Portuguese Engineering Association Prize for the best 1995 student at the Universidade de Aveiro, the 1998 Student Paper Competition (third place) presented at the IEEE Microwave Theory and Techniques Society (IEEE MTT-S) International Microwave Symposium (IMS), and the 2000 Institution of Electrical Engineers (IEE), U.K., Measurement Prize.

José Carlos Pedro (S'90–M'95–SM'99) was born in Espinho, Portugal, in 1962. He received the Diploma and Doctoral degrees in electronics and telecommunications engineering from the Universidade de Aveiro, Aveiro, Portugal, in 1985 and 1993, respectively.

From 1985 to 1993, he was an Assistant Lecturer with the Universidade de Aveiro, and a Professor since 1993. He is currently a Senior Research Scientist with the Instituto de Telecomunicações, Universidade de Aveiro, as well as a Full Professor. He has authored or coauthored several papers appearing in international journals and symposia. He coauthored *Intermodulation Distortion in Microwave and Wireless Circuits* (Artech House, 2003). His main scientific interests include active device modeling and the analysis and design of various nonlinear microwave and opto-electronics circuits, in particular, the design of highly linear multicarrier PAs and mixers.

Dr. Pedro is an associate editor for the IEEE TRANSACTIONS ON MICROWAVE THEORY AND TECHNIQUES and is also a reviewer for the IEEE Microwave Theory and Techniques Society (IEEE MTT-S) International Microwave Symposium (IMS). He was the recipient of the 1993 Marconi Young Scientist Award and the 2000 Institution of Electrical Engineers (IEE) Measurement Prize.